Program Digest, 2019 IEEE International Ultrasonics Symposium (IUS)
Glasgow, Scotland, October 6-9, 2019

A Free Plate Model Could Predict Ultrasonic Guided Waves Propagation in a 3D Printed Skull Phantom

Jialiang Gao[1], Qi Chen[1], Chen Jiang[1], Bo Hu[1], Jianqiu Zhang[1], Kailiang Xu*[1,2], Dean Ta[1,2]
[1] Department of Electronic Engineering, Fudan University, Shanghai, China
[2] Zhuhai Fudan Innovation Institute, Zhuhai, Guangdong, China

***Abstract*—Ultrasonic guided waves have been used to assess the quality of long cortical bone. Skull as a shell-structure, it may also support ultrasonic guided waves propagation. In this study, we used a free plate model to analyze the guided waves propagation in skull phantom and identified the guided modes. Simulation was performed using finite-difference time-domain (FDTD) method and the experiment was carried out on a 3D printed skull phantom and a plate phantom. The experimental dispersion trajectories were obtained using two-dimensional Fourier transform (2D-FT). No significant difference can be found between the results obtained from the plate and the skull phantoms, which illustrated that the Lamb theory used in long cortical bone could also be a proper model for analyzing guided modes in human skull.**

Keywords—Ultrasonic guided waves, Skull, Free plate mode, Dispersion curves

I. Introduction

As a common waveguide, plate or tubular structure can support the propagation of ultrasonic guided waves. Such characteristic have been widely employed in industrial ultrasonic non-destructive testing for its long-distance propagating characteristic. The cortical bone has a solid plate-like structure which also supports the propagation of guided waves [1]. In recent years, the ultrasonic guided waves have been successfully used to measure the elasticity of long cortical bone as well as to evaluate cortical thickness [3], cortical bone fracture [4], osteoporosis [6] and fatigue [7] etc.

Similar to the long cortical bone, as a shell-structure, skull may also support ultrasonic guided waves propagation. Understanding the interaction of ultrasound waves with skull would contribute to achieving focused ultrasound therapy deep inside human brain [9]. Recent studies have reported the observation of ultrasonic guided waves in human skull slice using photoacoustic, which shows that guided wave theory has a prospect for the evaluation of cortical skull bone [11]. However, the proper model for the guided waves propagated in the skull still need to be investigated.

In this study, a skull phantom is designed in a curvature-plate geometry, whose shape was derived from the CT data of a human skull. The skull phantom was made from photopolymer using stereolithography. Another plate phantom was made with the same material to verify the feasibility and effectiveness of applying the ultrasonic Lamb wave theory in the plate structure to human skull. The experiment was carried out using a programmable ultrasound array platform in the phantoms while simulation was performed using finite-difference time-domain (FDTD) method. In signal processing, two-dimensional Fourier transform (2D-FT) was used to characterize the dispersive energy of guided modes in frequency-wavenumber (f, k) domain, and the results are further compared with theoretical dispersion curves obtained using the plate model.

II. Materials and Methods

A. Lamb Wave Theory

Lamb wave is a general term for ultrasonic guided waves propagating in a plate or layered solid medium [13]. In a free plate with a thickness of $2h$, the Lamb wave propagation can be obtained by

$$\tan(qh) / \tan(ph) = -4k^2pq / (k^2-q^2)^2 \tag{1a}$$

$$\tan(qh) / \tan(ph) = -(k^2-q^2)^2 / 4k^2pq \tag{1b}$$

where k is the wavenumber, which is the ratio of angular frequency w to phase velocity c_p. The coefficients p and q are given by:

$$p^2 = w^2 / c_l^2 - k^2 \quad q^2 = w^2 / c_s^2 - k^2 \tag{2}$$

where c_l is the longitudinal velocity and c_s is the shear velocity. According to the distribution characteristics of guided waves in space, Lamb waves can be divided into symmetric modes (S_n, n = 0, 1, 2, …) described by equation (1a) and antisymmetric modes (A_n, n = 0, 1, 2, …) described by equation (1b).

B. Phantom

The CT data of the skull are obtained from the open source medical datasets of the University of Iowa (https://mri.radiology.uiowa.edu/visible_human_datasets.html). The relatively regular part of the skull (all of the frontal and the parietal and part of the occipital) was preserved and a vertical section in the direction of the line through the center of the occipital (i.e., the Z direction in Fig. 1) was made to obtain a two-dimensional (2D) skull contour. Because the overall thickness of the skull is not uniform (with the thickness range of about 2 mm-8 mm), the correction is made on the inner boundary to obtain a 2D skull slice model with an average thickness of 2.5 mm. Then the slice is expanded in the z direction into a curving plate-like structure, as shown in Fig. 1.

This work was supported by the National Natural Science Foundation (11525416, 11974081, 11827808 and 11604054), Natural Science Foundation of Shanghai (19ZR1402700), Shanghai Municipal Science and Technology Major Project (2017SHZDZX01) and State Key Laboratory of ASIC and System Project (2018MS004). *Corresponding author, Kailiang Xu, e-mail: xukl@fudan.edu.cn.

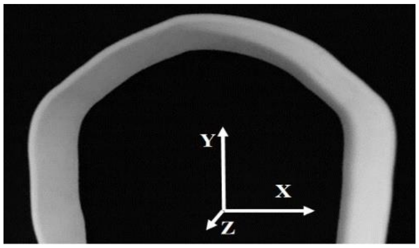

Fig. 1. The 3D printed Skull phantom

The 3D skull phantom is made from photopolymer using stereolithography, and a flat plate model with the same thickness was printed as a comparative sample imitating long cortical bone.

A standard rectangular parallelepiped model block (20 mm×25 mm×30 mm) was prepared as a sample to measure the material parameters of the phantom. Ultrasonic transmission method was used to measure the shear and longitudinal velocities [14]. The density is obtained by the ratio of mass to volume. The shear velocity, the longitudinal velocity and the density of the photopolymer are of 1129.01m/s, 2462.27 m/s and 1186.76 kg/m^3, respectively.

C. Simulation

Simulation was performed on the skull model using a 2D-FDTD system written in Matlab code. The perfect match layer (PML) was applied to eliminate boundary reflection at both ends of the skull [15].The material parameter are listed in TABLE I.

TABLE I. MATERIAL PARAMETERS OF THE SKULL MODEL

Material parameters	Skull phantom	Air
ρ (kg/m^3)	1186.76	1.29
λ (MPa)	4169	0.148
μ (MPa)	1513	0

The Lame coefficients λ and μ of the phantom are calculated from the density, the shear velocity c_s and the longitudinal velocity c_l.

$$\mu = c_s^2 \rho \qquad \lambda + 2\mu = c_l^2 \rho \tag{3}$$

D. Experiment Setup

The experiments were carried out by using the Verasonics Ultrasound Muti-channel Research Platform. a single-cycle sine wave with the frequency of 1 MHz was generated using an arbitrary waveform generator (Agilent 33220a, USA) and transmitted into the skull phantom through a power amplifier (AG 1021, T&C Power Conversion, Inc, USA). A 1.0 MHz single transducer was used as the emitter and a 22 linear-array with the central frequency of 1.0 MHz, bandwidth of 0.5-1.5MHz and pitch size of 0.675mm was used as the receiver.

III. RESULTS

The simulated array signals are processed using the 2D-FT method [16]. As shown in Fig. 2, the dispersion energy can be obtained in frequency-wavenumber (f, k) domain.

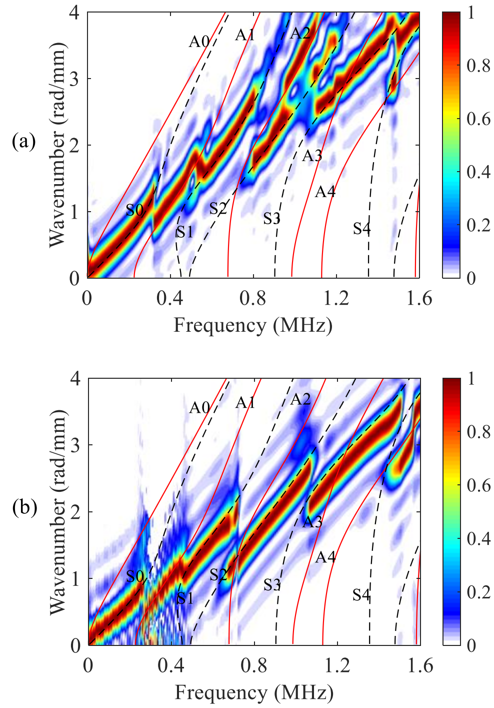

Fig. 2. Simulated Results. The (f, k) dispersion energy calculated using 2D-FT in (a) plate model and (b) skull model.

The theoretical dispersion curves computed using Rayleigh-Lamb equation were plotted in red solid lines (asymmetric modes, A_n mode) and black dashed lines (symmetric modes, S_n mode). S_0, A_1, S_1, A_2, S_2, S_3 and S_4 modes were obtained in simulated signals of the plate model while S_0, A_1, S_1, S_2, S_4 modes were obtained in the skull model.

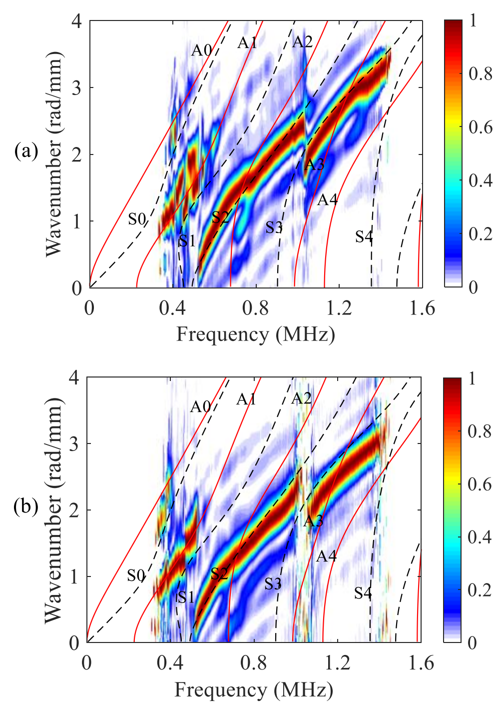

Fig. 3. Phantom results. The (f, k) dispersion energy calculated using 2D-FT in (a) a plate phantom and (b) a skull phantom.

The extracted dispersion curves in the phantom experiments are shown in Fig 3. In both phantoms, A_1, S_2 and S_3 modes were obtained. Similar to the simulated results, the dispersion energy extracted in the frequency-wavenumber (*f, k*) domain presents a good agreement with the corresponding theoretical dispersion curves.

IV. Discussion

Comparing the simulation with the phantom experiments, both of them obtained A_1, S_2 and S_3 modes, while S_0, S_1 and A_4 modes obtained in the simulation disappeared in the phantom experiment. Restricted by the bandwidth of the linear-array, part of low-frequency S_0 and A_4 modal energy cannot be measured in experiments. The energy distribution of S_1 mode is close to that of the A_1 mode, so mode overlapping occurred in the (*f, k*) domain.

In the experiments, no significant differences can be found between the results of the plate and the skull phantoms. Both present a good accordance with the theoretical dispersion curves. This illustrated that skull curvature may have limited impacts on guided wave propagation, and that the plate model which has been used to interpret the guided waves in the long cortical bone, could also be a proper model for analyzing the guided modes in human skull.

V. Conclusion

In In this study, ultrasonic guided waves were excited in a 3D-printed skull phantom. The dispersion curves were extracted in the frequency-wavenumber (*f, k*) domain by 2D-FT method. The dispersion curves obtained basing on the plate model present a good accordance with the experimental results. It is illustrated that skull curvature may have limited impacts on guided wave propagation, and the Lamb wave theory could also be used for interpreting the guided waves propagation in human skull. In future work, the sparse SVD method [17] will be applied to improve the dispersion curves extraction of the ultrasonic guided waves in the skull. Further experiments with real human skull are encouraged.

References

[1] D. Pereira, G. Haiat, J. Fernandes and P. Belanger, “Effect of intracortical bone properties on the phase velocity and cut-off frequency of low-frequency guided wave modes (20–85 kHz),” *The Journal of the Acoustical Society of America*, vol. 145, no. 1, pp. 121-130, Jan. 2019.

[2] N. Bochud, Q. Vallet, J.G. Minonzio and P. Laugier, “Predicting bone strength with ultrasonic guided waves,” *Scientific reports*, vol. 7, 43628, Mar. 2017.

[3] V. Kilappa, K. Xu, P. Moilanen, E. Heikkola, D. Ta and J. Timonen, “Assessment of the fundamental flexural guided waves in cortical bone by an ultrasonic axial-transmission array transducer,” *Ultrasound in Medicine and Biology*, vo. 39, no.7, pp. 1223-1232, July 2013.

[4] K. Xu, D. Ta, R. He, Y. X. Qin and W. Wang, “Axial transmission method for long bone fracture evaluation by ultrasonic guided waves: simulation, phantom and in vitro experiments,” *Ultrasound in Medicine and Biology*, vo. 40, no. 4, pp. 817-827, Apr. 2014.

[5] K. Xu, D. Liu, D. Ta, B. Hu, and W. Wang, “Quantification of guided mode propagation in fractured long bones,” *Ultrasonics*, vol. 54, no. 5, pp. 1210-1218, Jul. 2014.

[6] J. G. Minonzio, N. Bochud, Q. Vallet, D. Ramiandrisoa, A. Etcheto, K. Briot, S. Kolta, C. Roux, and P. Laugier, “Ultrasound‐based estimates of cortical bone thickness and porosity are associated with non‐traumatic fractures in postmenopausal women: A pilot study,” *Journal of Bone and Mineral Research*, vol. 34, no. 9, pp. 1585-1596, Sep. 2019.

[7] T. Falardeau and P. Belanger, “Ultrasound tomography in bone mimicking phantoms: Simulations and experiments,” T*he Journal of the Acoustical Society of America*, vol. 144, no. 5, pp. 2937-2946, Nov. 2018.

[8] L. Bai, K. Xu, D. Li, D. Ta, L. H. Le, and W. Wang, “Fatigue evaluation of long cortical bone using ultrasonic guided waves,” *Journal of Biomechanics*, vol. 77, no. 12, pp. 83-90, Aug. 2018.

[9] Pichardo, Samuel, Vivian W. Sin, and Kullervo Hynynen, “Multi-frequency characterization of the speed of sound and attenuation coefficient for longitudinal transmission of freshly excised human skulls,” *Physics in Medicine and Biology*, vol. 56, no. 1, pp. 219-251, Dec. 2010.

[10] G. Pinton, J.F. Aubry, E. Bossy, M. Muller, M. Pernot and M. Tanter, “Attenuation, scattering, and absorption of ultrasound in the skull bone,” *Medical physics*, vol. 39, no. 139, pp. 299-307, Jan. 2012.

[11] H. Estrada, J. Rebling, and D. Razansky, “Prediction and near-field observation of skull-guided acoustic waves,” *Physics in Medicine and Biology*, vol. 62, no. 12, pp. 4728-4740, May 2017.

[12] H. Estrada, S. Gottschalk, M. Reiss, V. Neuschmelting, R. Goldbrunner, and D. Razansky, “Observation of guided acoustic waves in a human skull,” *Ultrasound in Medicine and Biology*, vol. 44, no. 11, pp. 2388-2392, Nov. 2018.

[13] J. L. Rose, “Waves in Plates”, in Ultrasonic Guided Waves in Solid Media, Cambridge, UK: Cambridge University Press, 2014, pp. 76-106.

[14] L. Peralta, X. Cai, P. Laugier, and Q. Grimal, “A critical assessment of the in-vitro measurement of cortical bone stiffness with ultrasound,” *Ultrasonics*, vol. 80, pp. 119-126, Sep. 2017.

[15] E. Bossy, and Q. Grimal, “Numerical methods for ultrasonic bone characterization,” in *Bone Quantitative Ultrasound*, Dordrecht, Netherlands: Springer, 2011, pp. 181-228.

[16] T. E. Michaels, J. E. Michaels and M. Ruzzene, “Frequency–wavenumber domain analysis of guided wavefields,” *Ultrasonics*, vol. 51, no. 4, pp. 452-466, May 2011.

[17] K. Xu, J. G. Minonzio, D. Ta, B. Hu, W. Wang and P. Laugier, “Sparse SVD method for high-resolution extraction of the dispersion curves of ultrasonic guided waves,” *IEEE Transactions on Ultrasonics, Ferroelectrics and Frequency Control*, vol. 63, no. 10, pp. 1514-1524, Jul. 2016.